

A microscopic view of the yielding transition in concentrated emulsions

E. D. Knowlton,^a D. J. Pine,^{*b} and L. Cipelletti,^{*c,d}

Received Xth XXXXXXXXXX 20XX, Accepted Xth XXXXXXXXXX 20XX

First published on the web Xth XXXXXXXXXX 20XX

DOI: 10.1039/b000000x

We use a custom shear cell coupled to an optical microscope to investigate at the particle level the yielding transition in concentrated emulsions subjected to an oscillatory shear deformation. By performing experiments lasting thousands of cycles on samples at several volume fractions and for a variety of applied strain amplitudes, we obtain a comprehensive, microscopic picture of the yielding transition. We find that irreversible particle motion sharply increases beyond a volume-fraction dependent critical strain, which is found to be in close agreement with the strain beyond which the stress-strain relation probed in rheology experiments significantly departs from linearity. The shear-induced dynamics are very heterogeneous: quiescent particles coexist with two distinct populations of mobile and ‘supermobile’ particles. Dynamic activity exhibits spatial and temporal correlations, with rearrangements events organized in bursts of motion affecting localized regions of the sample. Analogies with other sheared soft materials and with recent work on the transition to irreversibility in sheared complex fluids are briefly discussed.

1 Introduction

Concentrated emulsions are viscoelastic materials, whose response to a mechanical perturbation depends both on the time scale and the amplitude of the perturbation.^{1,2} For a small applied stress or strain, concentrated emulsions behave as a solid on short time scales, but eventually flow as liquids on much longer time scales. Similarly, a transition from a predominantly solid-like to a mostly liquid-like behavior is observed when varying the amplitude of an applied strain, for example. An elastic response is observed up to a critical strain, typically a few percent, beyond which the emulsion yields and flows as a fluid. This yielding transition has an obvious importance for the countless everyday materials based on emulsions, *e.g.* in the food and personal care industry.

At a more fundamental level, the yielding transition of emulsions and other amorphous soft materials (concentrated colloids, foams, clays, pastes) has been extensively investigated as a prototypical manifestation of the (un)jamming transition³ and to understand plasticity in amorphous solids. One of the key question concerns the relationship between the rhe-

ological behavior and the microscopic rearrangements that are ultimately responsible for the macroscopic mechanical behavior. While in crystalline solids it has been firmly established that yielding is mediated by defects,^{4,5} identifying the microscopic elementary events leading to flow in amorphous materials is more challenging, due to their disordered structure.

Theoretical work has introduced the notion that localized, non-affine rearrangements are the building blocks of the transition from elastic deformation to plastic flow, for example, in the free volume approach of the flow defects of Ref. [6], or in the shear transformation zones of Ref. [7]. Subsequent simulations^{8–13} and experiments^{14–17} have confirmed that plastic events are localized, focusing predominantly on the stationary flow resulting from an applied constant strain rate.

The microscopic behavior of amorphous viscoelastic materials under an oscillatory shear has received less attention, in spite of the fact that cyclic perturbations are widely used in rheological¹⁸ and fatigue tests in material science. Hébraud and coworkers¹⁹ have probed the microscopic dynamics of concentrated emulsions under a sinusoidal shear deformation using diffusing wave spectroscopy²⁰ (DWS), a dynamic light scattering technique in the limit of strong multiple scattering. The main finding of this work was that plastic rearrangements are highly heterogeneous: the majority of the sample is deformed elastically and recovers its microscopic configuration after a full cycle, while a small fraction of drops undergo irreversible rearrangements. These rearrangements repeatedly affect the same subpopulation of drops. As the applied strain, γ , is increased, the fraction of rearranged sample increases. Quite surprisingly, at the yielding transition (as identified by

^a Department of Chemical Engineering, University of California Santa Barbara, Santa Barbara, CA 93106, USA

^b Center for Soft Matter Research, Department of Physics, New York University, New York, NY 10003, USA. E-mail: pine@nyu.edu

^c Department of Chemical and Biomolecular Engineering, Polytechnic School of Engineering, New York University, New York, NY 11201, USA. E-mail: pine@nyu.edu

^d Université Montpellier 2, Laboratoire Charles Coulomb UMR 5221, F-34095, Montpellier, France. E-mail: luca.cipelletti@univ-montp2.fr

^e CNRS, Laboratoire Charles Coulomb UMR 5221, F-34095, Montpellier, France.

rheology) more than 90% of the sample still behaves elastically at the microscopic level. Petekidis *et al.*²¹ have applied the same method to glassy suspensions of colloidal hard spheres. They also find heterogeneous plastic rearrangements, but the populations of mobile and immobile (after one full cycle) particles were found to evolve with time. As for the emulsions, the fraction of particles undergoing plastic events increases with γ . Interestingly, the sharpness of the yielding transition was found to depend on colloid volume fraction, ϕ : the higher ϕ , the more abrupt the transition.

Although these works pioneered the investigation of the yielding transition at a microscopic level, they suffered to some extent from the difficulties inherent to the interpretation of DWS data. The method provides information on the *average* microscopic dynamics, but provides no direct information on the heterogeneous nature of the rearrangements. Various assumptions have to be made, which cannot be verified independently. For example, it is extremely difficult to discriminate between a partial loss of correlation of the scattered light due to substantial motion of a small fraction of the sample, or, conversely, stemming from more restrained displacements affecting a larger fraction of the sample. Furthermore, no information on the temporal organization of the rearrangements can be obtained, since the intensity correlation function measured in DWS usually needs to be averaged over time. This is an important limitation, since numerical simulations²² have shown that rearrangements occur intermittently in a three-dimensional Lennard-Jones amorphous solid, a model system for soft particles. In this respect, optically microscopy is an attractive alternative to DWS, and it has been recently used to probe the yielding transition under oscillatory shear in both colloids²³ and emulsions²⁴. The authors of Ref. [24] focus mainly on the motion of drops that *do* recover their initial position after a full shear cycle; however, an interesting side observation that supports the conclusions of¹⁹ is the fact that only a small fraction of the sample undergoes irreversible rearrangements, even close to the macroscopic yielding transition.

Oscillatory strain experiments have also been considered under the perspective of the transition from reversible to irreversible motion. In Ref. [21] it was already noted that cyclic deformations may be fully reversible because the hydrodynamics equations at low Reynolds number are invariant under time reversal, leading to a ‘reversible viscous distortion’. Experiments on relatively diluted, non-Brownian suspensions have explored systematically this effect^{25,26}, showing that a transition exists between a low- γ absorbing state where particles fully recover their initial position after one shear cycle, and an irreversible state, where particles undergo diffusive motion as the result of collisions with other colloids for large enough strain amplitudes. In Refs. [25, 26] the hallmarks of a second-order transition have been observed: the diffusivity increases gradually beyond a critical strain γ_c separating the

reversible and irreversible regimes, and the time required to attain a stationary state seemingly diverges as γ approaches γ_c from both below and above. Remarkably, a similar reversible-irreversible transition has been reported recently for concentrated systems of interacting particles, both numerically²⁷ (three-dimensional Lennard-Jones glass) and experimentally (grains²⁸ and repulsive colloids in two dimensions²⁹). This is particularly surprising given that in Refs. [25, 26] the reversible state is due to the absence of particle interactions at small γ , an ingredient that is clearly missing in Refs. [27–29]. Quite intriguingly, the authors of a very recent experimental study on a dilute system with long-range interactions³⁰ reach an opposite conclusion: a reversible-irreversible transition is observed, but the transition is first-order. These contrasting results indicate that our understanding of sheared amorphous systems is still far from complete and calls for new investigations.

In this paper, we report on an optical microscopy study of the dynamics of concentrated emulsions submitted to an oscillatory shear. We present data for five volume fractions, from just above random close packing to $\phi = 0.88$, where the drops are highly compressed. For each ϕ , we perform experiments at a variety of strain amplitudes, both below and above the yielding transition as inferred from rheology. Each experimental run consists of several thousands of shear cycles, thereby allowing a thorough investigation of the spatio-temporal behavior of plasticity. Finally, microscopy observations are systematically compared to the results of rheological tests, in order to establish a connection between the microscopic dynamics and the mechanical response across the yielding transition. The rest of the paper is organized as follows: in Sec. 2 we describe the emulsion preparation, the shear cell, and the image analysis procedure. Section. 3 presents our results, which are discussed and summarized in Sec. 4.

2 Materials and methods

2.1 Emulsion preparation

We use oil in water emulsions, where the oil phase is polydimethylsiloxane, PDMS (Petrarch) and the dispersing phase a mixture of water and glycerol, to partially match the refractive index of the drops. The content of glycerol is fine-tuned by optimizing the optical contrast for microscopy observations. Since the optical properties of the emulsions depend on compression, different amounts of glycerol were added depending on the emulsion volume fraction. For $\phi < 0.80$, the glycerol/water ratio is 40% w/w; it is 20% for $0.80 \leq \phi \leq 0.85$, while for the most concentrated emulsion ($\phi = 0.88$) the ratio is 10%. The drops are stabilized by a non-ionic surfactant. Various surfactants have been tested in order to achieve good stability and avoid wall slip under shear. The best re-

sults are obtained with TMN-10 (2,6,8 trimethylnonyl ethoxide, Union Carbide), at a concentration of 1.7% w/w in the aqueous phase.

The emulsions are prepared as described in Refs. [31, 32]. The method consists of preparing a crude emulsion (‘premix’) by slowly dripping PDMS in the aqueous phase in the presence of an excess of surfactant, while gently stirring. The premix is then sheared at a high strain rate (typically, 1500 s^{-1}) in a couette cell, to reduce the drop size down to $2.4 \mu\text{m}$, with a relative size polydispersity of 20%, as measured by static light scattering (Malvern Mastersizer). Solvent is added to reduce the surfactant to the desired final value, and the emulsion is finally concentrated to the desired volume fraction by centrifugation. The precise value of ϕ is determined by weighting the fraction of oil left after evaporating the dispersing phase in a vacuum oven operated at 70°C .

2.2 Microscopy under shear and image analysis

We use a custom-made shear cell and a Nikon Eclipse TE-2000 inverted microscope to visualize shear-induced rearrangements. The shear cell design is based on that by Petekidis *et al.*²¹ In brief, the sample is confined in a gap of thickness $e = 100 \mu\text{m}$ between two parallel borosilicate glass plates. The lower plate is a coverslip, the upper one a standard microscopy slide. To avoid wall slip, both plates are roughened using wet sandpaper and lapping compounds, resulting in a roughness of about $1 - 2 \mu\text{m}$, as estimated by optical microscopy. A small window of about 1 mm^2 is left un-roughened on the coverslip, to allow for visualization. A lever system allows the upper and lower plate to be moved in opposite directions, with a stagnation plane located approximately midway in the gap. A cyclic strain is imposed by a piezoelectric actuator (PiezoMechanik GmbH), whose position controller is driven by a sinusoidal signal (frequency $f = 1 \text{ Hz}$) issued from an ultra-low distortion function generator (Stanford Research Systems). The strain values quoted in the following are obtained from $\gamma = y_0/e$, with y_0 the amplitude of the relative motion of the two plates.

The shear cell is fixed on the stage of an inverted microscope equipped with differential interference contrast (DIC) optics and an oil-immersion 100x objective and oil-immersion condenser. The depth of field is $0.5 \mu\text{m}$, much smaller than the drop size, and the imaged plane lays about $10 \mu\text{m}$ from the coverslip. Images are taken with a Matrox Helios frame grabber and a Dalsa Pantera TF 1M60 CCD camera, triggered so as to take a strobed movie at one frame per shear cycle. The image size is 1024×1024 pixels and the pixel size corresponds to $0.12 \mu\text{m}$ in the sample. Before any experiment at a given strain and volume fraction, the sample is presheared at a high strain, typically 250-300% at a frequency of 1 Hz. The strain amplitude is then reduced to the target value and at least

300 cycles are imposed at the final γ before starting the image acquisition.

Figure 1(a) shows a representative image of an emulsion at $\phi = 0.65$, the lowest volume fraction that was investigated. Tracking the motion of individual drops is very difficult due to size polydispersity and because the drop shapes in compressed emulsions are not spherical. These difficulties could be attenuated by using larger drops, but this would limit the number of drops that can be visualized. We therefore use a different approach and quantify motion using image correlation velocimetry (ICV),³³ a cross-correlation method similar to particle imaging velocimetry.³⁴ Each image is divided in regions of interest (ROI) of size 32×32 pixels²; a displacement vector $\Delta\mathbf{r}(\mathbf{R}, t, \tau)$ is assigned to a ROI centered in \mathbf{R} by maximizing the spatial cross-correlation between the intensity pattern of the ROI at time t and that of an image taken at time $t + \tau$. More precisely, $\Delta\mathbf{r}$ is obtained with sub-pixel resolution by fitting the peak of $\text{Corr}(\Delta; \mathbf{R}, t, \tau)$ by a paraboloid, where

$$\text{Corr}(\Delta; \mathbf{R}, t, \tau) = \langle I(\mathbf{r}, t) I(\mathbf{r} + \Delta, t + \tau) \rangle_{\mathbf{R}} - \langle I(\mathbf{r}, t) \rangle_{\mathbf{R}} \langle I(\mathbf{r} + \Delta, t + \tau) \rangle_{\mathbf{R}}, \quad (1)$$

where \mathbf{r} is a pixel coordinate, Δ a spatial shift whose components are integer numbers of pixels, and where $\langle \cdot \cdot \rangle_{\mathbf{R}}$ indicates an average over pixels belonging to the ROI centered in \mathbf{R} . In the following, time will be expressed in numbers of shear cycles and only the dynamics over one cycle will be discussed, corresponding to $\tau = 1$ in Eq. (1). The red box in Fig. 1(b) shows the size of one of the ROIs used by the image correlation algorithm: it typically contains about three drops. As it will be discussed in the following, even at the largest applied strains the typical displacements over one shear cycle are relatively small, of order $0.2 \mu\text{m}$. The yellow line in Fig. 1(b) visualizes such a displacement in the y direction. In principle, one may distinguish between motion along the direction parallel or perpendicular to the imposed strain (x and y , respectively). We find no significant difference between the dynamics in the two directions, as also seen for colloids in Ref. [23]: in the following we discuss the results for the y component of the displacement, which would be zero in the absence of plastic rearrangements, even if the images were not perfectly strobed with the shear cycle. By inspecting the results obtained for very low applied strains, where no irreversible rearrangements are expected to occur, we estimate the error on the determination of the ROI displacement to be on the order of 0.05 pixel at most.

3 Results

We start by discussing the macroscopic mechanical behavior of the emulsions¹, as measured by oscillatory rheology in a 50-mm cone-and-plate geometry. Figure 2 shows the strain

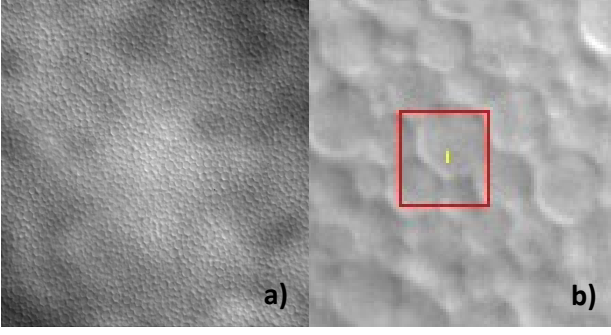


Fig. 1 (a) DIC microscopy image of an emulsion at $\phi = 0.65$. The field of view is $122.9 \times 122.9 \mu\text{m}^2$. The long-range intensity modulations are due to the illumination through a roughened microscopy slide. (b) zoom on a portion of the image shown in (a): the drops are clearly visible. The red square shows the size ($3.84 \times 3.84 \mu\text{m}^2$) of the ROIs used to measure the drop displacements by an image correlation algorithm. The yellow line corresponds to the y component of the rms drop displacement after one shear cycle, for the largest applied shear amplitude, $\gamma = 7.88\%$.

dependence of the elastic, G' , and loss, G'' , moduli, measured at an oscillation frequency $f = 1$ Hz. Although we show here data for a single volume fraction, $\phi = 0.83$, qualitatively similar behavior is observed for the whole range over which experiments were performed, $0.64 \leq \phi \leq 0.88$. As the applied strain increases, G'' grows, indicating that dissipative processes, presumably due to drop rearrangements, become increasingly likely. However, the emulsions retain an overall solid-like behavior, with G' larger than G'' and only weakly dependent on γ . Beyond a few percent of applied strain amplitude, G' drops significantly and G'' grows until $G' = G''$ at a ‘fluidization’ strain $\gamma_f \approx 20\%$. For $\gamma > \gamma_f$, both moduli decrease with strain, but the loss modulus dominates, indicating fluid-like behavior. It should be emphasized that the transition from solid-like to fluid-like behavior is a very smooth one, extending over at least one decade in strain amplitude. Because of its smooth nature, several alternative ways are routinely used to define the yielding transition in concentrated emulsions. One criterion is based on the crossing point of the moduli, γ_f , introduced above. A more stringent criterion is to identify the strain amplitude beyond which significant deviations from the linear regime are observed. To this end, we show in Fig. 2 the γ dependence of the shear stress σ measured during the imposed strain sweep (open circles and right axis). Two power-law regimes are clearly visible, as evidenced by the straight lines. The crossover between the initial linear regime and the large- γ , sublinear growth of the stress defines a rheological yield strain, $\gamma_{y,r} = 6.4\%$, which occurs substantially earlier than the fluidization crossover.

In order to investigate the yielding transition at a micro-

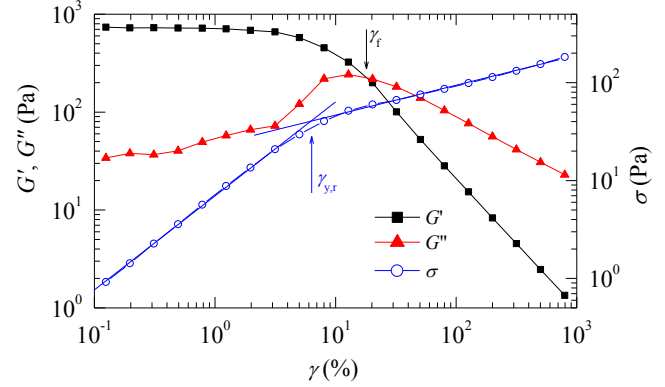


Fig. 2 Left axis and solid symbols: shear moduli vs. strain amplitude γ , measured by oscillatory rheology at a frequency of 1 Hz, for an emulsion at volume fraction $\phi = 0.83$. The cross-over or fluidization strain γ_f is defined by the intersection of G' and G'' (black arrow). Right axis and open symbols: shear stress vs. γ . The rheological yield strain $\gamma_{y,r}$ is defined by the intersection of the two lines describing the behavior of σ at small and large strain, respectively (blue arrow).

scopic level, we measure the displacement field over one shear cycle, as a function of both emulsion volume fraction and strain amplitude. We show in Fig. 3(a) $\sqrt{\langle \Delta y^2 \rangle}$, the rms displacement in the y direction, as a function of γ for five emulsions with volume fraction ranging from $\phi = 0.65$, just above the jamming transition, up to $\phi = 0.88$, where the emulsion is highly compressed. Data are averaged over all ROIs and over the duration of each experiment. A sharp increase of $\sqrt{\langle \Delta y^2 \rangle}$ is observed beyond a ϕ -dependent critical strain. This has to be contrasted to the much gentler transition observed by rheology (Fig. 2). For $\phi \geq 0.74$, the transition is particularly abrupt. For example, at $\phi = 0.74$ $\sqrt{\langle \Delta y^2 \rangle}$ jumps by one order of magnitude when the strain increases by less than 1%. For the sake of comparison, we consider the variation of $\tan \delta = G''/G'$ around $\gamma_{y,r}$, as $\tan \delta$ is often used to characterize the transition from solid-like to fluid-like behavior.¹⁸ For the system shown in Fig. 2, we find that $\tan \delta$ increases by a decade over a much wider interval of strain amplitude, $\Delta\gamma \approx 16\%$. Interestingly, the yielding transition detected at a microscopic level becomes less sharp as the jamming transition is approached from above. This can be seen in Fig. 3(a), where for the most diluted sample a one-decade growth of $\sqrt{\langle \Delta y^2 \rangle}$ occurs over a strain interval of about 3%, three times larger than for samples at $\phi \geq 0.74$. This suggests that the nature of the yielding transition may depend on the distance from the jamming transition.

We define the microscopic yield strain γ_y as the strain beyond which the rms displacement exceeds $10^{-2} \mu\text{m}$ (dotted

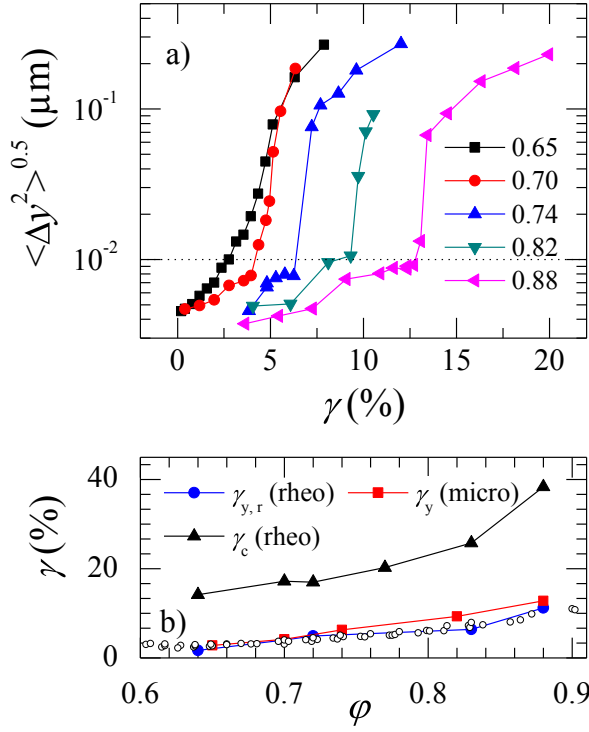


Fig. 3 (a) Shear dependence of the rms displacement per shear cycle in the y direction, perpendicular to the applied shear. Data are labeled by the emulsion volume fraction. The dotted line is the threshold used to define the microscopic yield strain, γ_y . (b) Volume fraction dependence of the yielding transition, as defined by various quantities. The small open symbols are rheology data taken from Ref. [1].

line in Fig. 3(a)). This threshold is chosen based on the behavior of the more concentrated samples, and is then used at all ϕ . The volume fraction dependence of γ_y is shown in Fig. 3(b), together with the two yield strains defined from rheological measurements, as discussed in reference to Fig. 2. Remarkably, we find that the yield strain inferred from microscopy measurements agrees very well with $\gamma_{y,r}$ defined by the onset of non-linear behavior in the stress-strain relation. This result is particularly surprising given that the sharpness of the transition is very different for microscopy and rheology. The rheological yield strain $\gamma_{y,r}$ has been shown to depend only marginally on sample details (drop size, composition, etc.), as shown by the open symbols in Fig. 3(b), taken from a comprehensive set of experiments by Mason *et al.*¹ This suggests that the behavior observed in our microscopy experiments should be quite general. It should be noted that at all volume fractions γ_y is much smaller than the rheological cross-over strain γ_c . Thus, a substantial increase in drop motion occurs well

before the sample is actually fully fluidized.

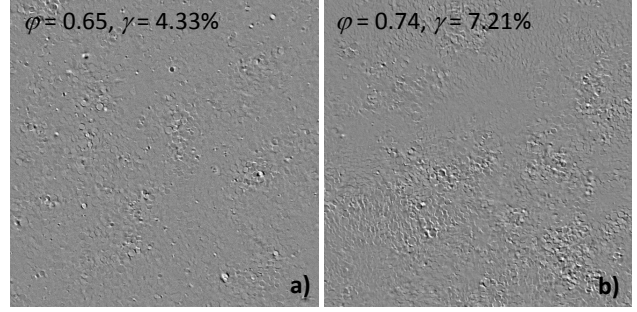


Fig. 4 Difference between two successive strobed images: regions where motion occurred show up as features brighter or dimmer than the average background, while immobile regions are featureless. For each sample, the applied strain is just above the yield strain γ_y .

While Fig. 3 quantifies the strain and ϕ dependence of the average dynamics, our microscopy experiments allow us to investigate in detail both the spatial and temporal distribution of the rearrangements responsible for the drop displacement. A convenient way to visualize the regions that have undergone rearrangements over one cycle is to inspect the difference between a pair of successive strobed images. Figure 4 shows the result of such image subtraction for two representative volume fractions and for strain amplitudes just above γ_y . Regions where no motion occurred appear identical in the pair of images, yielding patches of uniform grey level in Fig. 4. By contrast, rearranged regions show up as contrasted zones, whose intensity changes from bright to dark along the contour of a displaced droplet. It is clear that the drop motion is spatially heterogeneous, with islands of mobile particles separated by quiescent patches.

To investigate quantitatively the heterogeneity of the dynamics hinted to by the images of Fig. 4, we calculate the probability distribution function of the drop displacement over one cycle, $P_y(\Delta y)$. Figure 5(a) shows P_y for a sample at $\phi = 0.74$: its features are representative of all samples at $\phi \geq 0.74$, for which the yielding transition is very sharp. We find that positive and negative displacements are equally likely; we therefore plot the data against $|\Delta y|$. Two well-separated sets of curves are visible. For strains smaller than the yield strain (solid symbols), the pdf's decay very rapidly to zero, implying that most of the drops are essentially quiescent. This is also shown in Fig. 5(b), where we plot the cumulative distribution function, $C_y(|\Delta y|) = \int_0^{|\Delta y|} P_y(u) du$. For $\gamma < \gamma_y = 6.32\%$, 98.5% or more of the drops move by less than $0.024 \mu\text{m}$, *i.e.* a mere one-hundredth of their size. By contrast, for $\gamma > \gamma_y$ (open symbols), motion on a much larger length scale is observed. As seen in Fig. 5(a), above the yield strain the pdf's are characterized by a two-step shape, with two distinct decays that

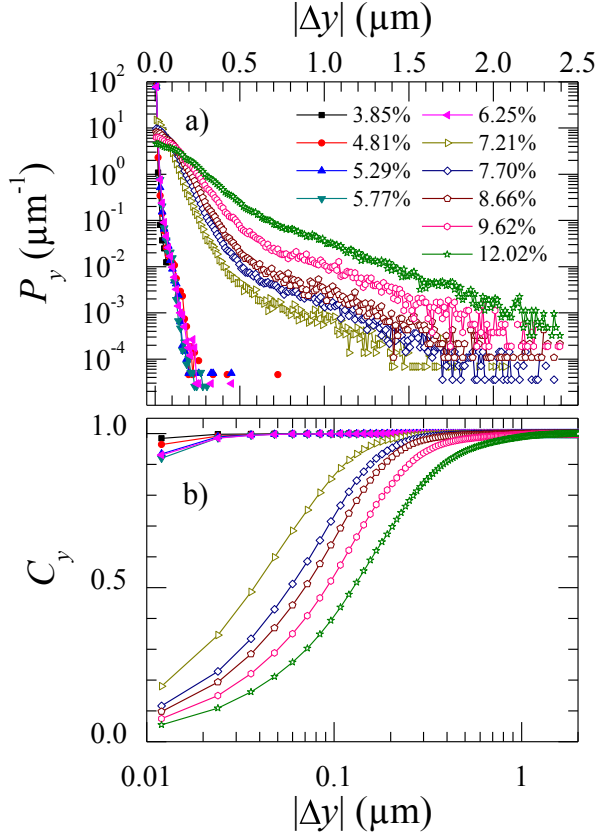


Fig. 5 (a) Probability distribution function of the drop displacements over one shear cycle, in the direction orthogonal to the applied strain, for an emulsion at $\phi = 0.74$. Curves are labeled by the amplitude of the applied strain. Solid (resp., open) symbols refer to γ below (resp., above) the yield strain γ_c . (b) Cumulative distributions obtained by integrating the probability distributions shown in the top panel.

appear as straight lines in a semilog plot. Thus, two populations of particles with different mobility coexist, which we shall refer to as the ‘mobile’ and ‘supermobile’ particles, each population being characterized by a nearly exponential distribution of displacements. It should be noted that a non-negligible fraction of particles still remain almost quiescent. Indeed, the cumulative distributions of Fig. 5(b) reveal that at $\gamma = 7.21\%$, just above the yielding transition, more than a third of the particles (34.6%) move less than $0.024 \mu\text{m}$, the restrained displacement typical of the vast majority of drops below γ_y . Even at the largest applied strain, $\gamma = 12.02\%$, more than 10% of the particles remain essentially quiescent. The persistence of a fraction of immobile droplets is consistent with the quiescent patches observed, at all strains, when subtracting pairs of consecutive images, as in Fig. 4. It is also consistent with previous experiments by both DWS¹⁹ and microscopy.²⁴

Figure 5(a) reveals the origin of the continuous growth of the rms displacement beyond the yielding transition seen in Fig. 3(a). As γ increases, two concomitant mechanisms lead to a larger average displacement. On the one hand, the typical displacement of the mobile particles grows, as indicated by the flattening of the first decay in the pdf’s. On the other hand, the fraction of supermobile particles increases, while their characteristic displacement remains roughly constant, as indicated by the fact that the large- $|\Delta y|$ tails of the distributions have nearly the same slope but are shifted upwards with increasing γ . By fitting the tail of the pdf’s to an exponential decay, $P_y \sim \exp(-|\Delta y|/\Delta_s)$, we find the characteristic displacement of the supermobile particles to be $\Delta_s = 0.31 \mu\text{m}$, where the quoted value has been obtained by averaging the results for $\gamma \geq 7.7\%$, which exhibit little variation with γ . Such a displacement corresponds to about 13% of the average drop size.

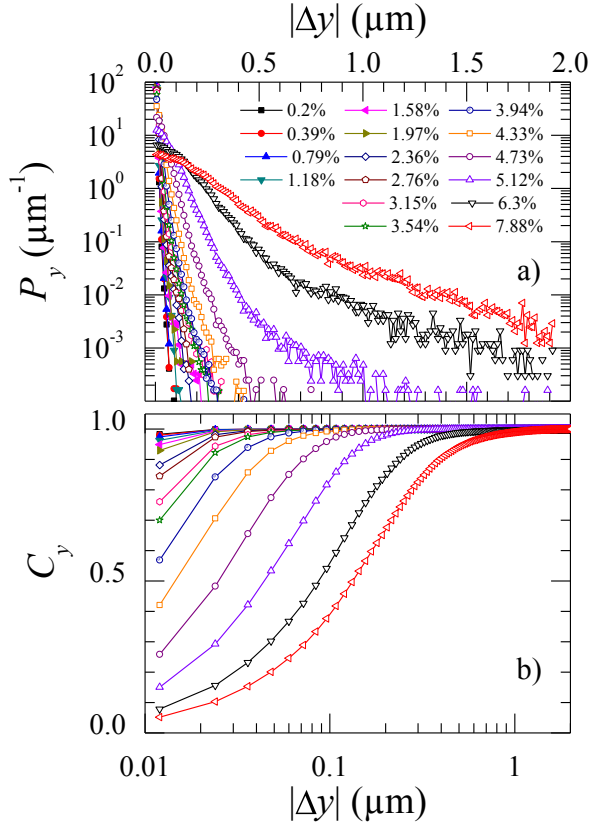


Fig. 6 (a) Probability distribution function of the drop displacements over one shear cycle, in the direction orthogonal to the applied strain, for an emulsion at $\phi = 0.65$. Curves are labeled by the amplitude of the applied strain. Solid (resp., open) symbols refer to γ below (resp., above) the yield strain γ_c . (b) Cumulative distributions obtained by integrating the probability distributions shown in the top panel.

Figure 6 shows the probability (a) and cumulative (b) distributions of the drop displacements for the most diluted sample ($\phi = 0.65$), for which the least sharp yielding transition was observed in Fig. 3. Consistent with a gentler transition, we find that both P_y and C_y evolve in a more continuous way with γ , as compared to the sample at $\phi = 0.74$ shown in Fig. 5: no clear separation in the two family of curves is observed. For the sample at $\phi = 0.70$, the behavior is intermediate between those shown in Figs. 5 and 6 (data not shown). In spite of the differences for $\gamma \leq \gamma_y$, the behavior beyond the yielding transition is very close for all samples, including the most dilute one shown in Fig. 6. Again we find that quiescent particles coexist with two distinct populations of mobile and supermobile droplets. Similarly to the case of the sample at $\phi = 0.75$, the typical displacement of the supermobile particles is insensitive to the amplitude of the applied strain, while the fraction of supermobile particles increases with γ , until the pdf exhibits almost a single exponential decay, for the largest γ . From an exponential fit to the tail of the pdfs at large γ , we obtain $\Delta_s = 0.35 \mu\text{m}$, comparable to the typical displacement of the supermobile particles measured at $\phi = 0.74$.

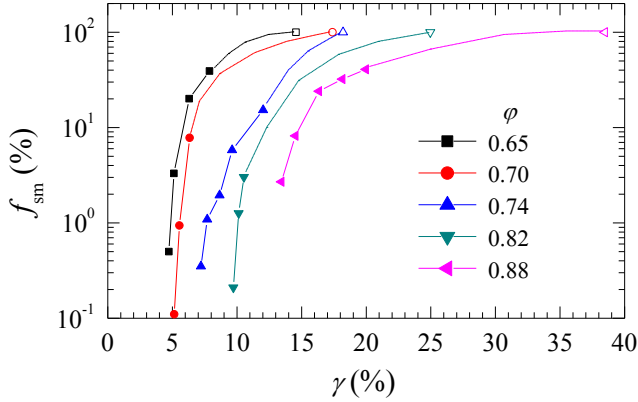


Fig. 7 Solid symbols: fraction f_{sm} of the “supermobile” drops, whose displacement falls in the the exponential tail of the probability distribution P_y , as discussed in the text. The abscissa of the open points correspond to the rheological crossover strain γ_f , where the sample is fluidized. The dotted lines are guides to the eye, consistent with the hypothesis that full fluidization may occur when all drops are supermobile, *i.e.* for $f_{\text{sm}} = 100\%$.

From a similar analysis performed on the pdfs for all investigated ϕ , we find that the typical displacement of the supermobile particles is $\bar{\Delta}_s = (0.26 \pm 0.07) \mu\text{m}$, where the average and the uncertainty are calculated over all experiments at large strain, regardless of ϕ . Quite intriguingly, the average Δ_s is about 11% of the drop size, close to the amplitude of particle motion leading to the melting of a crystalline solid according to Lindemann’s criterion³⁵, for which the typical

threshold is around 15% of the particle spacing. Although the supermobile particles are just a small fraction of all drops at the yielding transition, their relative number increases rapidly as γ exceeds γ_y (see the raise of the tails of P_y in Figs. 5(a) and 6(a)). The question naturally arises as whether the full fluidization of a sheared emulsions occurs when all (or at least the majority of) the particles are supermobile, which would constitute an analogous of the Lindemann’s criterion for an amorphous solid. To test this idea, we plot as solid symbols in Fig. 7 the fraction of supermobile particles, as a function of the amplitude of the applied strain, where a particle is taken to be supermobile if its displacement over one shear cycle exceeds $\bar{\Delta}_s$. We add to the plot the points that would correspond to a full fluidization when all particles are supermobile (open symbols): by definition, their ordinate is 100%, while their abscissa is γ_f , the fluidization strain beyond which $G'' > G'$. The dotted lines are a guide to the eye, connecting the solid and open symbols. While our experiments do not allow this extension of Lindemann’s criterion to be definitively confirmed, the data are sufficiently compelling to call for more experiments in a wider range of applied strains.

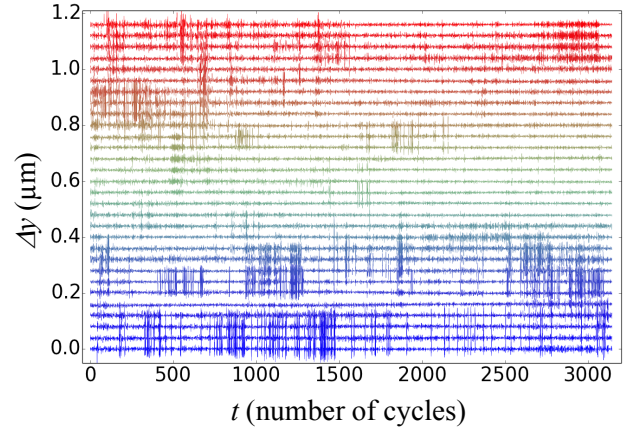


Fig. 8 Temporal evolution of Δy , measured for 30 ROIs aligned along a vertical line spanning the whole height of the microscopy images. Data for $\phi = 0.7$ and $\gamma = 6.25\%$, just below the yielding transition. Each curve has been offset by $0.04 \mu\text{m}$ with respect to the previous one for visibility.

We now turn to the spatio-temporal organization of the droplet motion. Figure 8 shows a set of time series of the drop displacement, $\Delta y(t, \mathbf{R})$, measured in 30 ROIs whose center \mathbf{R} is aligned along a vertical line spanning the whole height of the microscopy images, for a sample at $\phi = 0.7$ and for $\gamma = 6.25\%$, just below the yielding transition. Two features strike the eyes: on the one hand droplet motion is not continuous in time, but rather proceeds by intermittent bursts of activ-

ity followed by quiescent periods. On the other hand, regions with correlated dynamical activity extend over several ROIs, since the time series for nearby ROIs exhibit a similar behavior. We go beyond this qualitative observations by measuring both the temporal and spatial correlations of the dynamics.

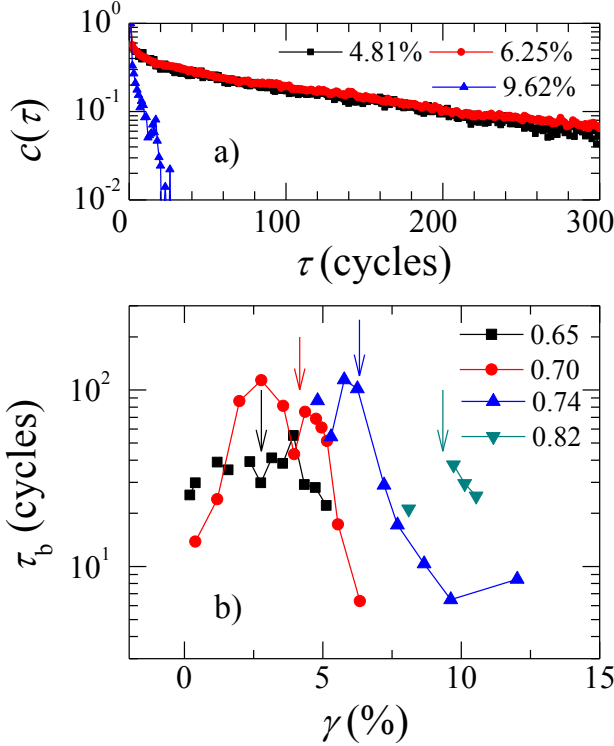


Fig. 9 (a) Time autocorrelation function of $|\Delta y(t)|$, for a sample at $\phi = 0.74$ and for the three strain amplitudes shown in the label. γ is well below, just below and well above the microscopic yield strain γ_c , respectively. (b) Strain dependence of the characteristic time of $c(\tau)$, for samples at $\phi \leq 0.82$, as indicated by the label. The autocorrelation functions for $\phi = 0.88$ are too noisy for a relaxation time to be extracted reliably. The arrows indicate the location of the microscopic yielding transition.

Temporal correlations are quantified by calculating

$$\tilde{c}(\tau) = \langle \langle |\Delta y(t, \mathbf{R})| |\Delta y(t + \tau, \mathbf{R})| \rangle_t \rangle_{\mathbf{R}} \quad (2)$$

where $\langle \dots \rangle_t$ and $\langle \dots \rangle_{\mathbf{R}}$ indicate averages over the experiment duration and the ROI location, respectively. Note that we calculate the autocorrelation of the absolute y displacement, rather than that of Δy itself. This is because we aim at capturing the duration of the activity bursts, better seen when the rapid and chaotic fluctuations around 0 of the displacement are suppressed. We find that $\tilde{c}(\tau)$ still contains significant noise contributions at time lags $\tau = 0$ and $\tau = 1$. We thus neglect the

first two points of $\tilde{c}(\tau)$ and study the normalized time autocorrelation function, defined as $c(\tau) = \tilde{c}(\tau)/\tilde{c}(2)$, for $\tau \geq 2$. Typical examples of c are shown in Fig. 9(a), for $\phi = 0.74$ and three strain amplitudes, well below, near to, and well above the yielding transition, respectively. We extract the characteristic decay time of the autocorrelation function, which we identify with the typical burst duration τ_b , from

$$\tau_b = \frac{1}{T-2} \int_2^T c(\tau) d\tau, \quad (3)$$

where T is the smallest delay for which c has decayed below 0.1. The strain dependence of τ_b is shown in Fig. 9(b), for various ϕ . For the largest volume fraction, $\phi = 0.88$, \tilde{c} decays very rapidly to a noisy base line, thus making our normalization procedure difficult to apply and preventing τ_b from being calculated. Overall, τ_b is quite large, from several cycles to more than 100 cycles: this highlights the need of performing long experiments in order to fully capture the temporal behavior of the rearrangements. On the other hand, the burst duration remains finite: this rules out the hypothesis that a given fraction of the drops are *always* immobile, while some of them are *always* rearranged, as proposed in the DWS experiments of [19]. It should be noted however that in Ref. [19] the average dynamics could only be measured over a period of 16 cycles: in most cases such a reduced time span is comparable to or shorter than τ_b , which would explain why the populations of mobile and immobile particles did not seem to be exchanged over time in the DWS experiments.

Spatial correlations of the dynamics are investigated by inspecting how similar are the displacement time series recorded in two locations of the sample, as a function of the location separation $\Delta \mathbf{r}$. We introduce the un-normalized spatial correlation $G_4(\Delta \mathbf{r})$, similar to those used to analyze heterogeneous dynamics in glass formers and granular media³⁶, and defined by

$$G_4(\Delta \mathbf{r}) = \langle \langle \Delta y(\mathbf{R}, t) \Delta y(\mathbf{R} + \Delta \mathbf{r}, t) \rangle_t \rangle_{\mathbf{R}}, \quad (4)$$

Note that G_4 compares not only the magnitude of the displacement, but also the *direction* along which it occurs, since the correlation is calculated for the y component, rather than for the modulus of the displacement. Thus, G_4 quantifies spatial correlations in a rather stringent sense, rather than just dynamical activity. We find that G_4 does not depend on the orientation of $\Delta \mathbf{r}$, *i.e.* that spatial correlations are isotropic, consistent with the observation that the plastic dynamics observed in our experiments are independent of the shear orientation. In the following we thus report the azimuthally-averaged G_4 , which we normalize by calculating

$$g_4(\Delta r) = a [G_4(\Delta r) - b]. \quad (5)$$

The coefficients a and b are chosen such that $g_4(\Delta r \rightarrow 0) = 1$, $g_4(\Delta r \rightarrow \infty) = 0$. In practice, b is obtained as the mean value

of G_4 for $\Delta r \geq 96 \mu\text{m}$, while a is obtained as the 0-th order term in a cumulant fit³⁷ to $G_4 - b$:

$$\ln[G_4(\Delta r) - b] = \ln a - \xi_y \Delta r + \Gamma_2(\Delta r)^2. \quad (6)$$

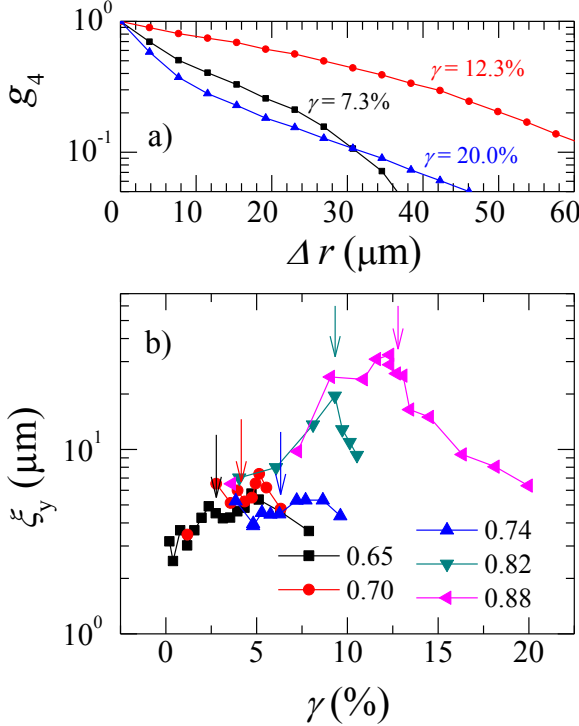


Fig. 10 (a) Spatial correlation of the dynamics (y component), for a sample at $\phi = 0.88$ and for the three strain amplitudes shown by labels. γ is well below, nearly at and well above the microscopic yield strain γ_c , respectively. (b) Strain dependence of the correlation length of the dynamics, obtained from fits to g_4 . Data are labeled by ϕ . The arrows indicate the location of the microscopic yielding transition.

Figure 10(a) shows g_4 for the most concentrated sample ($\phi = 0.88$), for three strain amplitudes well below, nearly at, and well above the yielding transition, respectively. At both small and large applied strain, the dynamics are correlated over a few microns, a distance comparable to a couple of drop sizes. By contrast, much long range spatial correlations of the dynamics are observed close to the microscopic yield strain. To test the generality of this behavior, we show in Fig. 10(b) for all samples the γ dependence of ξ_y , the characteristic range of the spatial correlations obtained from cumulant fits, Eq. (6). For $\phi \leq 0.74$, the behavior of ξ_y is very different from that inferred from Fig. 10(a): at the lowest volume fractions, the range of correlated motion remains modest and quite insensitive to γ over the full range of applied strain amplitudes.

At larger ϕ , by contrast, ξ_y grows significantly as the applied strain approaches the yield value, where spatial correlations may extend up to 20 particle sizes. At even larger strain, ξ_y decreases. Inspection of movies of the strobed images reveal the origin of this non-monotonic behavior. As γ is increased, coordinated motion of increasingly large patches of particles is observed, until essentially all the sample moves, but in an increasingly disordered way at very high γ .

4 Discussion and conclusions

The first important finding of our experiments is the steep increase of the drop mobility over a restricted range of applied strains, shown in Fig. 3(a), which contrasts with the very smooth yielding transition observed by rheology (Fig. 2). This behavior likely depends on the fact that, in a compressed emulsion, local motion of a few drops is inevitably propagated elastically to a large number of neighbors. This would favor a nearly on-off behavior, where either the sample is (almost) quiescent everywhere, or it is significantly rearranged (almost) everywhere. Two observations support this view. First, as ϕ decreases, the transition become less sharp, presumably because this mechanism is less efficient just above random close packing, where elastic propagation of a local rearrangement is screened. Second, a similar trend was reported for sheared colloidal glasses.²¹ It should be noted that the colloidal glasses of Ref. [21] were prepared at lower volume fractions than our emulsions. Consistent with the proposed scenario, the yielding transition is found to be overall smoother for colloidal glasses than in the experiments reported here. In spite of the differences in the sharpness of the microscopic and rheological yielding transitions, the two critical strains, $\gamma_{y,x}$ and γ_y obtained from the two techniques agree remarkably well. This result appears to be robust with respect to the criterion used to define the microscopic yield strain, since a similar conclusion was also reached by analyzing the DWS intensity correlation functions in Ref. [19]. It should be emphasized that γ_y is much smaller than the fluidization strain γ_f : substantial plastic rearrangements occur well before the sample flows.

Another important finding is the fact that the dynamics are heterogenous, with almost quiescent particles coexisting with mobile particles. Indeed, as discussed in reference to Figs. 5 and 6, a significant fraction of drops undergo very restricted motion even around or above the yield strain. This is consistent with the interpretation of the DWS measurements proposed in Ref. [19]. However, the microscopy experiments allow a more refined picture of the drop dynamics to be drawn. A very peculiar distribution of the amplitude of the drop motion is seen, as evidenced by the exponential tails of P_y in Figs. 5(b) and 6(b). We recall that for diffusive motion P_y should be Gaussian, a behavior clearly incompatible with our data. Exponential tails in the pdf's of the displacement have

been consistently observed in glassy and jammed systems, *e.g.* in sheared foams,³⁸ grains,³⁹ and colloids,²³ and even in simulations of molecular glass formers.⁴⁰ A general mechanism has been proposed to explain these exponential tails,⁴⁰ based on the idea that particles undergo discontinuous jumps. This picture seems compatible with the nature of the rearrangements in our emulsions. However, the double exponential tail measured here points to a more complex behavior, which will need further experiments to be fully understood, for example by studying systematically the spatial and temporal distribution of the supermobile particles.

The droplet dynamics show complex spatio-temporal organization. While such heterogenous behavior is overall consistent with what inferred in Ref. [19], an important difference concerns the life time of the active regions, which in the optical microscope experiments is found to be finite, albeit very long: τ_b can be as long as hundreds of cycles, which highlights the necessity of performing experiments over a very large number of cycles. Both the time scale and the spatial range of dynamical correlations have a non-monotonic behavior with γ , reaching a maximum at a strain comparable to the yield strain, except for the lowest ϕ , for which little variation of τ_b and ξ_y is observed when varying γ . In recent simulations of a sheared Lennard-Jones glass,²² a monotonic increase of the range of spatial correlations with γ was reported. Unfortunately, the largest tested strain, $\gamma = 6\%$, was relatively limited, so that it is difficult to conclude as whether or not a non-monotonic behavior would be observed at even larger strains. Non-monotonic spatial correlations as a function of ϕ have been also reported for the spontaneous dynamics of colloids close to jamming⁴¹. Close to random close packing, spatial correlations of the dynamics extend over a few particles at most, similarly to Ref. [22] and in analogy to the dynamics of other glassy or jammed systems, both driven and at rest.³⁶ As ϕ grows, the range of spatial correlations significantly grows, as seen in Fig. 10(b). The same trend, with similar values of ξ (expressed in numbers of drops) was observed in Ref. [16]. This analogy is remarkable, given that the experiments of Goyon *et al.* are performed in a steady flow regime, where in our case the largest ξ_y are measured around γ_y , when the sample has still a predominantly solid-like behavior.

Finally, it is interesting to consider the experiments presented here from the perspective of the ongoing debate on the transition from reversibility to irreversibility in driven complex fluids.^{25–30} A first point to keep in mind is that no fully reversible state is actually observed here, since even at the lowest applied strains some dynamics are observed. This is also true, at least on a finite time scale, for most of the work on systems of interacting particles where the existence of a reversible regime was advocated.^{27–30} This has to be contrasted with the experiments on dilute, non-interacting particles,^{25,26} where a genuine fully reversible state was observed. Concern-

ing the nature of the transition, for our system we find contrasting results according to ϕ . Close to random close packing, the smooth increase of the average drop displacement and the continuous evolution of P_y with γ are suggestive of a second order-transition, but no strong growth of temporal and spatial quantities is seen around the transition, in contrast to the findings of Refs. [25, 26]. At higher volume fraction, both τ_b and ξ_y grow significantly when approaching the yielding transition, but the partitioning between mobile and (almost) immobile particles and the sharpness of the transition are rather suggestive of a first-order transition, as in Ref. [30]. Overall, it seems that the nature of the yielding transition depends on the distance from the jamming transition and that the analogy with the transition to irreversibility discussed for diluted suspensions^{25,26} may be of limited relevance.

Several questions are left open by the work presented here and will deserve further investigation. The existence of a Lindemann's criterion for amorphous solids discussed in relation to Fig. 7 is appealing, but certainly needs additional experiments at larger γ to be fully assessed. A second research direction would be exploring the dependence of the dynamics on time delay, τ . While exploring motion after one full shear cycle, as discussed here, is an essential starting point, particularly relevant for the comparison with rheology data, it is clear that much is to be learned by analyzing how particle displacement grows with time. A related question concerns the length scale dependence of the dynamics. While numerical works generally suggest that plastic rearrangements lead to diffusive dynamics, very recent experiments on a sheared colloidal polycrystal have shown that the network of defects relaxes *ballistically* under an oscillatory shear.⁴² It would be interesting to investigate the nature of the dynamics in concentrated emulsions, for which ballistic dynamics have been reported in the past for a sample submitted to compressional stress in a centrifuge.⁴³

Acknowledgments

This work was supported by U.S. National Science Foundation (Grant No. CTS-0221809) and CNES. LC thanks NYU Center for Soft Matter Research for supporting his stay at NYU. We acknowledge fruitful discussions with L. Berthier.

References

- 1 T. G. Mason, J. Bibette and D. A. Weitz, *Journal of Colloid and Interface Science*, 1996, **179**, 439–448.
- 2 T. G. Mason, M. D. Lacasse, G. S. Grest, D. Levine, J. Bibette and D. A. Weitz, *Physical Review E*, 1997, **56**, 3150–3166.
- 3 A. Liu and S. Nagel, *Nature*, 1998, **396**, 21–22.

- 4 L. B. Chen, C. F. Zukoski, B. J. Ackerson, H. J. M. Hanley, G. C. Straty, J. Barker and C. J. Glinka, *Physical Review Letters*, 1992, **69**, 688–691.
- 5 S. Biswas, M. Grant, I. Samajdar, A. Haldar and A. Sain, *Sci. Rep.*, 2013, **3**, year.
- 6 F. Spaepen, *Acta Metallurgica*, 1977, **25**, 407–415.
- 7 M. L. Falk and J. S. Langer, *Physical Review E*, 1998, **57**, 7192–7205.
- 8 R. Y. Onuki and A., *EPL (Europhysics Letters)*, 1997, **40**, 61.
- 9 K. Miyazaki, D. R. Reichman and R. Yamamoto, *Physical Review E*, 2004, **70**, 011501.
- 10 A. Lemaitre and C. Caroli, *Physical Review Letters*, 2009, **103**, 065501.
- 11 L. Bocquet, A. Colin and A. Ajdari, *Physical Review Letters*, 2009, **103**, 036001.
- 12 M. Tsamados, *Eur. Phys. J. E*, 2010, **32**, 165–181.
- 13 K. Martens, L. Bocquet and J.-L. Barrat, *Physical Review Letters*, 2011, **106**, 156001.
- 14 R. Besseling, E. Weeks, A. B. Schofield and W. C. K. Poon, *Physical Review Letters*, 2007, **99**, 028301–028301.
- 15 P. Schall, D. A. Weitz and F. Spaepen, *Science*, 2007, **318**, 1895–1899.
- 16 J. Goyon, A. Colin, G. Ovarlez, A. Ajdari and L. Bocquet, *Nature*, 2008, **454**, 84–87.
- 17 P. Jop, V. Mansard, P. Chaudhuri, L. Bocquet and A. Colin, *Physical Review Letters*, 2012, **108**, 148301.
- 18 R. G. Larson, *The structure and rheology of complex fluids*, Oxford University Press, New York, 1999.
- 19 P. Hébraud, F. Lequeux, J. P. Munch and D. J. Pine, *Physical Review Letters*, 1997, **78**, 4657–4660.
- 20 D. A. Weitz and D. J. Pine, in *Dynamic Light scattering*, ed. W. Brown, Clarendon Press, Oxford, 1993, pp. 652–720.
- 21 G. Petekidis, A. Moussaid and P. N. Pusey, *Physical Review E*, 2002, **66**, 051402.
- 22 N. V. Priezjev, *Physical Review E*, 2013, **87**, 052302.
- 23 D. Chen, D. Semwogerere, J. Sato, V. Breedveld and E. R. Weeks, *Physical Review E*, 2010, **81**, 011403.
- 24 J. Clara-Rahola, T. A. Brzinski, D. Semwogerere, K. Feitosa, J. C. Crocker, J. Sato, V. Breedveld and E. R. Weeks, *ArXiv e-prints*, 2012, 1204.5110.
- 25 D. J. Pine, J. P. Gollub, J. F. Brady and A. M. Leshansky, *Nature*, 2005, **438**, 997–1000.
- 26 L. Corte, P. M. Chaikin, J. P. Gollub and D. J. Pine, *Nat Phys*, 2008, **4**, 420–424.
- 27 D. Fiocco, G. Foffi and S. Sastry, *Physical Review E*, 2013, **88**, 020301.
- 28 S. Slotterback, M. Mailman, K. Ronaszegi, M. van Hecke, M. Girvan and W. Losert, *Physical Review E*, 2012, **85**, 021309.
- 29 N. C. Keim and P. E. Arratia, *Soft Matter*, 2013, **9**, 6222–6225.
- 30 R. Jeanneret, *Ph.D. thesis*, Université Paris Diderot, 2014.
- 31 T. G. Mason and J. Bibette, *Langmuir*, 1997, **13**, 4600–4613.
- 32 C. Mabilie, V. Schmitt, P. Gorria, F. L. Calderon, V. Faye, B. Deminiere and J. Bibette, *Langmuir*, 2000, **16**, 422–429.
- 33 P. T. Tokumaru and P. E. Dimotakis, *Experiments in Fluids*, 1995, **19**, 1–15.
- 34 J. Westerweel, *Measurement Science & Technology*, 1997, **8**, 1379–1392.
- 35 F. A. Lindemann, *Physik. Z.*, 1910, **11**, 609–612.
- 36 *Dynamical Heterogeneities in Glasses, Colloids and Granular Media*, ed. L. Berthier, G. Biroli, J. Bouchaud, L. Cipelletti and W. van Saarloos, Oxford University Press, New York, 2011.
- 37 D. E. Koppel, *Journal of Chemical Physics*, 1972, **57**, 4814–4820.
- 38 M. E. Möbius, G. Katgert and M. van Hecke, *Europhysics Letters*, 2010, **90**, 44003.
- 39 G. Marty and O. Dauchot, *Physical Review Letters*, 2005, **94**, 015701.
- 40 P. Chaudhuri, L. Berthier and W. Kob, *Physical Review Letters*, 2007, **99**, 060604.
- 41 P. Ballesta, A. Duri and L. Cipelletti, *Nature Physics*, 2008, **4**, 550–554.
- 42 E. Tamborini, L. Cipelletti and L. Ramos, *ArXiv e-prints*, 2013, 1311.1996.
- 43 L. Cipelletti, L. Ramos, S. Manley, E. Pitard, D. A. Weitz, E. E. Pashkovski and M. Johansson, *Faraday Discuss.*, 2003, **123**, 237–251.